MANUSCRIPT DOUBLEDECK2_V.B2.TEX
Preprint typeset using LaTeX style emulateapj v. 5/2/11

arXiv:1407.2272v1 [astro-ph.SR] 8 Jul 2014

SLOW RISE AND PARTIAL ERUPTION OF A DOUBLE-DECKER FILAMENT. II MODELING BY A DOUBLE FLUX ROPE EQUILIBRIUM

BERNHARD KLIEM[1,2,3,4], TIBOR TÖRÖK[5], VIACHESLAV S. TITOV[5], ROBERTO LIONELLO[5], JON A. LINKER[5], RUI LIU[6,7], CHANG LIU[7], AND HAIMIN WANG[7]

Submitted: May 29, 2014

ABSTRACT

Force-free equilibria containing two vertically arranged magnetic flux ropes of like chirality and current direction are considered as a model for split filaments/prominences and filament-sigmoid systems. Such equilibria are constructed analytically through an extension of the methods developed in Titov & Démoulin (1999) and numerically through an evolutionary sequence including shear flows, flux emergence, and flux cancellation in the photospheric boundary. It is demonstrated that the analytical equilibria are stable if an external toroidal (shear) field component exceeding a threshold value is included. If this component decreases sufficiently, then both flux ropes turn unstable for conditions typical of solar active regions, with the lower rope typically being unstable first. Either both flux ropes erupt upward, or only the upper rope erupts while the lower rope reconnects with the ambient flux low in the corona and is destroyed. However, for shear field strengths staying somewhat above the threshold value, the configuration also admits evolutions which lead to partial eruptions with only the upper flux rope becoming unstable and the lower one remaining in place. This can be triggered by a transfer of flux and current from the lower to the upper rope, as suggested by the observations of a split filament in Paper I (Liu et al. 2012). It can also result from tether-cutting reconnection with the ambient flux at the X-type structure between the flux ropes, which similarly influences their stability properties in opposite ways. This is demonstrated for the numerically constructed equilibrium.

Subject headings: Instabilities—Magnetohydrodynamics (MHD)—Sun: coronal mass ejections (CMEs)—Sun: filaments, prominences—Sun: magnetic topology

1. INTRODUCTION

The magnetic structure of solar prominences (filaments if observed on the disk) is one of the major debated subjects in solar physics: a flux rope and a sheared loop arcade are being controversially discussed (e.g., Mackay et al. 2010). An extension of the flux rope concept is suggested to be relevant in some cases by the analysis of a "double-decker" filament in Liu et al. (2012), hereafter Paper I. The filament, located in active region (AR) 11093, consisted of two main branches and experienced a partial eruption, ejecting only the upper branch into a coronal mass ejection (CME), on 2010 August 7. The clear vertical separation of the filament branches prior to eruption and the stability of the lower branch in the course of the eruption both suggest that the filament may have formed in a double flux rope structure. An alternative explanation in terms of a single flux rope situated above an arcade which contains the lower filament branch is also possible, but has the disadvantage that basically different magnetic structures for the two filament branches are implied. These two configurations are illustrated in Figure 1, and their possible formation mechanisms and relevance for the event considered in Paper I will be discussed in Section 5. The formation of both filament branches within a single flux rope or within an arcade is far less likely, as it requires two special conditions to be satisfied simultaneously: the trapping of filament material at two clearly separated heights and the formation of the flare current sheet in the course of the eruption at an intermediate height.

A striking phenomenon observed during the slow-rise phase of the upper filament branch in AR 11093 prior to its eruption was the transfer of material from the lower to the upper branch, occurring in several episodes. Assuming dominantly horizontal field orientation in the filament, a corresponding transfer of flux is implied. This may have caused the eruption by producing an imbalance between the flux in the upper branch and the ambient flux (e.g., Su et al. 2011), lifting the upper branch into the torus-unstable height range (Kliem & Török 2006; Kliem et al. 2013).

Zhu & Alexander (2014) describe a very similar event in AR 11475 on 2012 May 9–10. The filament consisted of two branches separated in height. Several discrete episodes of mass transfer from the lower to the upper branch occurred in the two days preceding the eruption of the upper branch into a CME, while the lower branch remained stable.

A double flux rope configuration was also suggested to exist prior to an eruption in AR 11520 on 2012 July 12 (Cheng et al. 2014). The event featured an erupting sigmoidal "hot channel" structure above a stable filament, similar in many respects to an eruption on 2010 August 1 investigated in Liu et al. (2010). Since this combination is not rare (e.g., Pevtsov 2002; Liu et al. 2007, 2008), the double flux rope structure may be more common than expected so far.

Employing two magnetohydrodynamic (MHD) modeling approaches, the present paper substantiates the suggestion

bkliem@uni-potsdam.de
[1] Institute of Physics and Astronomy, University of Potsdam, Karl-Liebknecht-Str. 24, 14476 Potsdam, Germany
[2] Yunnan Observatories, Chinese Academy of Sciences, Kunming 650011, China
[3] Mullard Space Science Laboratory, University College London, Holmbury St. Mary, Dorking, Surrey RH5 6NT, UK
[4] College of Science, George Mason University, Fairfax, VA 22030, USA
[5] Predictive Science, Inc., San Diego, CA 92121, USA
[6] CAS Key Laboratory of Geospace Environment, University of Science and Technology of China, Hefei 230026, China
[7] Space Weather Research Laboratory, Center for Solar-Terrestrial Research, NJIT, Newark, NJ 07102, USA

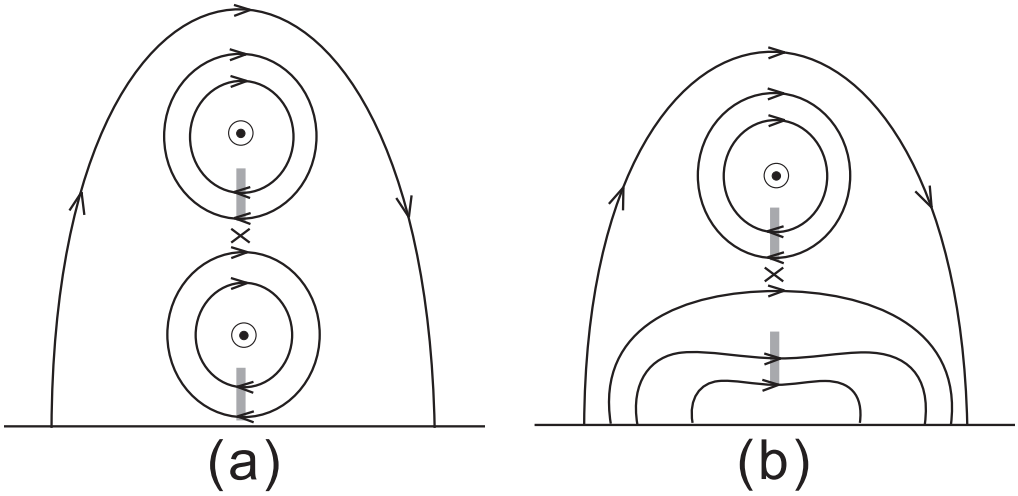

Figure 1. Cartoon illustrating the cross section of the two double-decker filament configurations suggested in Paper I: (a) double flux rope equilibrium; (b) flux rope above a sheared arcade. The axial field of both filament branches points in the same direction (out of the plane in the specific case analyzed in Paper I). The HFT is indicated by a small cross. Slabs of gray color indicate the filament body trapped in dipped field line sections.

that a double flux rope configuration can be consistent with the long-term stability of the filaments studied in Paper I, Zhu & Alexander (2014), and Cheng et al. (2014) during their slow rise phase, and with the partial eruptions. This also introduces new scenarios for partial filament eruptions. For some events these may be an alternative to the dynamical splitting and partial expulsion of a single, originally purely O-type flux rope whose top part has become unstable while the bottom part remains line-tied in the photosphere (Gibson & Fan 2006). In such a configuration the flux splits only after the main acceleration of the ejection has commenced.

We restrict the consideration to the case that the flux ropes are of like chirality, with the axial field component pointing into the same direction, as suggested by the relevant events quoted above. This can be expected to be the typical situation in split filaments that form side by side in the same filament channel and have common or close end points. The axial (toroidal) currents in the ropes then point in the same direction implying an attractive force between them.

The existence of a stable double flux rope equilibrium is not trivial if the ropes are relatively close to each other so that the force between them is comparable to or larger than the force exerted by the ambient field. Perturbations will then trigger a pinching of the X-type magnetic structure between the ropes, which in general is a hyperbolic flux tube (HFT; see Titov et al. 2002). The subsequent reconnection at the formed current sheet will start redistributing the magnetic flux between the ropes and the ambient field. This may cause the perturbation to grow, eventually merging the ropes or pushing them apart, depending on the properties of the configuration and perturbation.

Using an extension of the Shafranov equilibrium of a single toroidal force-free flux rope (Shafranov 1966; Titov & Démoulin 1999), we first demonstrate the existence, stability, and instability of an equilibrium containing two vertically arranged force-free flux ropes in bipolar external field (Section 2). We find that the external field's toroidal (shear) component is a key parameter controlling the stability of the configuration if the ropes are relatively close to each other. We also demonstrate that a scenario of current and flux transfer from the lower to the upper rope, which resembles the flux transfer indicated by the observations in Paper I and Zhu & Alexander (2014), leads to instability of the upper flux rope only.

In Section 3 we describe an MHD simulation which exhibits the formation of a split flux rope during the slow-rise phase of a modeled filament eruption. Different from the model by Gibson & Fan (2006), this timing corresponds to the observations of the double-decker filaments presented in Paper I and in Zhu & Alexander (2014).

2. STABILITY AND INSTABILITY OF A DOUBLE FLUX ROPE EQUILIBRIUM

2.1. *Construction of the Equilibrium*

We build on the construction of an approximate analytical equilibrium of a toroidal force-free flux rope in bipolar current-free external field described in Titov & Démoulin (1999, hereafter TD99), done in two steps. First, the "external equilibrium" of the rope in a given simple (axisymmetric) external poloidal field $B_{\rm ep}$ is determined by balancing the Lorentz force of the flux rope current in the field $B_{\rm ep}$ with the Lorentz self-force (hoop force) of the current. Then an approximate "internal equilibrium" of the current channel in the core of the rope is constructed by matching the expressions for a straight force-free current channel in each cross section of the toroidal channel to the external field at its surface.

A second, larger flux rope, lying in a concentric arrangement in the same plane as the first rope, can easily be added at a sufficiently large distance, such that its influence on the external equilibrium of the first rope is negligible. The second rope can then be constructed in the same way as a single rope, except that the known poloidal field of the first rope must be added to the external poloidal field in determining the external equilibrium of the second rope. This very simple approximation yields equilibria that readily relax to a numerical equilibrium very near to the analytical one if the ratio of the major radii is not smaller than ≈ 4.

In order to find equilibria of two flux ropes with smaller distance, the construction of the external equilibrium in TD99 can straightforwardly be generalized (see below). Doing so also for the internal equilibrium is a very involved task, which we do not aim to pursue here. However, applying the expressions for the internal equilibrium without modification to each channel individually yields an acceptable approximation down to ratios of the major radii of ≈ 2.5. Subsequent numerical MHD relaxation quickly adjusts the internal equilibrum

of the ropes and, supported by line tying in the photospheric boundary, yields a nearby force-free numerical equilibrium in the stable part of the parameter space.

We now consider the external equilibrium of two concentric toroidal current channels lying in a plane. Here the relevant poloidal field is the superposition of the external poloidal field, $B_{\rm ep}$, and the poloidal field by the other current channel, B_I, where I is the total toroidal (ring) current of the channel. In TD99 the external poloidal field is due to a pair of auxiliary magnetic charges $\pm q$ on the symmetry axis of the torus at distance $\pm L$ from the torus plane (or simply the field connecting the corresponding "sunspots" in the photospheric plane); we will also refer to this field component as B_q. Using subscripts 1 and 2 to denote quantities of the inner (lower) flux rope FR1 and outer (upper) flux rope FR2, respectively, we have the following dependencies on the flux rope currents: $F_{I_{1,2}} \propto I_{1,2}^2$ for the Lorentz self-force; $F_{q_{1,2}} \propto I_{1,2}$ for the force by the field from the magnetic charges; and $F_{B_{1\leftrightarrow 2}} \propto I_1 I_2$ for the force due to the field of the other current channel. The resulting force equations,

$$0 = F_{I_1} + F_{q_1} + F_{B_{2\to 1}} = b_1 I_1^2 + c_1 I_1 + e_1 I_1 I_2 \qquad (1)$$

$$0 = F_{I_2} + F_{q_2} + F_{B_{1\to 2}} = b_2 I_2^2 + c_2 I_2 + e_2 I_1 I_2\,, \qquad (2)$$

can easily be solved for I_1 and I_2, given the geometry ($R_{1,2}$, $a_{1,2}$, d, L) and the strength of the field B_q, set by q and L. Here R and a denote major and minor torus radius, respectively, and d is the depth of the torus center below the photospheric plane. The expressions of the coefficients $b_{1,2}$, $c_{1,2}$, and $e_{1,2}$ can be found in TD99 (their Equations 5, 4, and 25, respectively). As in TD99, an axisymmetric external toroidal field $B_{\rm et}$ of arbitrary strength can be superposed. It is provided by an auxiliary line current I_0 running along the symmetry axis of the tori. Given the geometry, q, and the currents I_0, I_1, and I_2, the equilibrium field can straightforwardly be computed as the superposition of B_q, $B_{\rm et}$, B_{I_1}, and B_{I_2}, using the expressions (16), (20), and (31) in TD99.

The resulting equilibrium is only a very crude approximation of the suggested interpretation of the double-decker filament in Paper I in terms of two flux ropes. Both ropes in the model must have toroidal shape, so that their footpoints are quite separate, different from the observed configuration. Moreover, the use of a line current as the source of the external toroidal field, dictated by the concentric arrangement of the tori, prevents us from realistically modeling an ejective eruption (a CME). Since the resulting $B_{\rm et}$ falls off only linearly with distance from the torus center, it enforces any eruption to remain confined for realistic values of its strength at the position of the flux ropes (Roussev et al. 2003; Török & Kliem 2005). On the other hand, the configuration allows us to demonstrate the existence of the suggested equilibrium, the instability of only the upper flux rope for certain parameter settings, and the key role of $B_{\rm et}$. This can be done for a geometry that matches the observed height relationships between the lower and upper filament branches at the apex points of the two flux ropes.

The double flux rope equilibrium is intrinsically less stable than the equilibrium of a single toroidal flux rope, due to the additional force between the ropes. To attain a stable force-free equilibrium in the absence of an external toroidal field, the ropes must be positioned sufficiently far apart, so that $F_{B_{1\leftrightarrow 2}}$ is small compared to $F_{q_{1,2}}$, and B_q must be relatively uniform, i.e., L must be large. The slope of the total poloidal field as a function of R then remains sufficiently small at the positions of both ropes, so that both are stable against vertical displacements (Kliem & Török 2006). Here we have to consider a situation with the flux ropes situated relatively close to each other and the sources of the field B_q also being relatively close (see below). In this case, an external toroidal field is required for stability. If one or both ropes are displaced by a perturbation, the compression of this field component will counteract the perturbation. Thus, the strength of the external toroidal field is a key parameter deciding between stability and instability of the configuration.

This is confirmed in the following subsection by MHD relaxation runs, which also show that a size ratio $R_2/R_1 \gtrsim 2.5$ is required for the analytical equilibrium to be close to a stable numerical one with the HFT lying not too close to the current channel in the lower rope. In the stable domain of parameter space, reconnection at the HFT remains very weak, just redistributing the fluxes to the extent needed to reach the nearby numerical equilibrium.

Prominence material in flux ropes is supposed to be trapped in dips of the field lines, i.e., it can occupy a slab-like volume extending between the bottom flux surface and the magnetic axis of the rope (Figure 1). The height measurements of the two filament branches on 2010 August 7 (Section 2.3 in Paper I) thus suggest apex heights of 12 and 36 Mm for the magnetic axis of FR1 and FR2, respectively, and an apex height of 25 Mm for the HFT (which is the bottom of the upper flux rope on the vertical line through the apex). The first two measurements are met, for example, by the choice $R_1 = 16$ Mm, $R_2 = 40$ Mm, $d = 4$ Mm. The third measurement can be met to a good approximation by the choice $a_1 = 4$ Mm, $a_2 = 6$ Mm, resulting in an HFT apex height of 23 Mm. We have chosen the current channels to be relatively thin, so that both possess a large aspect ratio, which guarantees relatively high precision in the construction of the equilibrium (TD99). Note that it is the larger cross section of the magnetic structure (the flux rope) which matters for the location of field line dips, not the cross section of the current channel. To have the HFT apex lying exactly at the estimated height of 25 Mm, we would have to choose $a_2 = 2$ Mm, smaller than a_1, which we consider neither appropriate nor necessary for the purpose of this study. Under the force-free constraint, the relatively small values of the minor radii imply relatively high values of the flux rope twists. Both ropes are stabilized against the helical kink mode by the external toroidal field. We set $L = 8$ Mm, corresponding to the observed distance of the main photospheric flux concentrations near the middle section of the filament studied in Paper I (see Figure 2 in Paper I).

2.2. *Numerical Simulations*

2.2.1. *Stable Configuration*

The resulting analytical equilibrium is used as initial condition in zero-beta MHD simulations in a cubic Cartesian box more than five times higher than FR2 and resolving the minor diameter of the current channel in FR1 by 35 grid cells. The initial density is specified as $\rho_0(\boldsymbol{x}) = |\boldsymbol{B}_0(\boldsymbol{x})|^{3/2}$, where $\boldsymbol{B}_0(\boldsymbol{x})$ is the initial magnetic field, so that the Alfvén velocity decreases slowly with height above the flux rope, as in the solar corona.

To check the equilibrium currents $I_{1,2}$ obtained from Equations (1–2), the field $B_{\rm et}$ is first set to a value somewhat (about 20 percent) below the value that provides stability. After normalizing by the apex height of FR1, $h_1 = R_1 - d$, and by

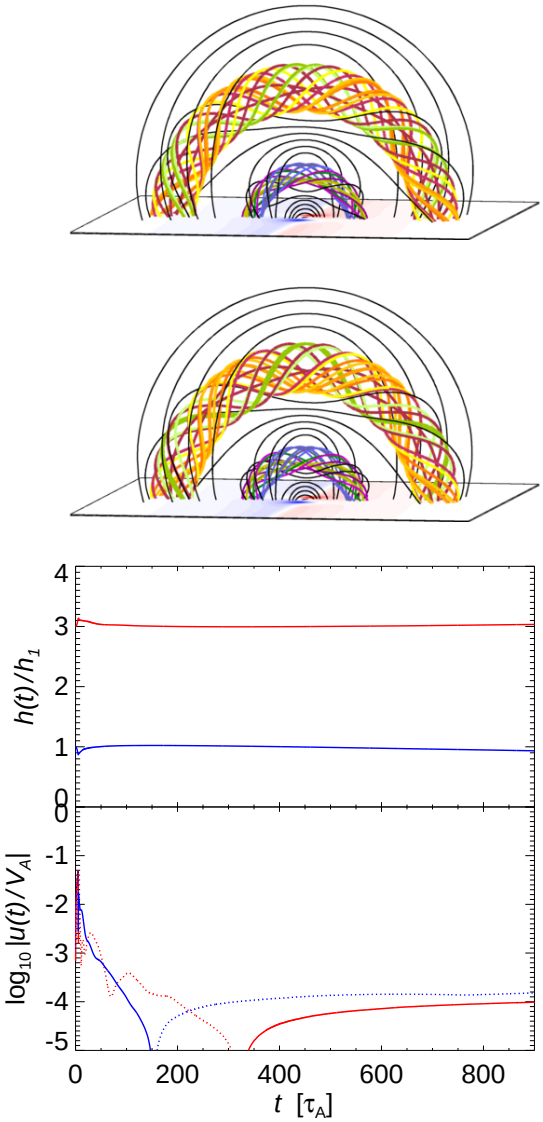

Figure 2. Field lines showing the two flux ropes in the stable analytical equilibrium with $B_{\rm et} = 1.7B_q$, slightly above the marginal stability value of the external toroidal field (top panel) and after numerical relaxation at $t = 645\tau_{\rm A}$ (middle panel). The field lines lie in flux surfaces near the surface of the current channels (slightly inside the channel for FR1). All black field lines pass through the vertical axis in the middle of the system, illustrating the apex heights of the two HFTs (below the lower rope FR1 and between FR1 and FR2) by the transition between downward and upward concave curvature. The magnetogram, $B_z(x, y, 0, t)$, is displayed in the bottom plane. The bottom panel shows height and velocity of the fluid elements at the apex points of the magnetic axes of the two ropes in the relaxation run. Due to the symmetry of the system, these fluid elements move only vertically. The relaxation run includes an initial velocity perturbation in small spherical volumes centered at the two apex points, applied up to $t = 5\ \tau_{\rm A}$. Downward velocities are shown dotted.

the corresponding Alfén time $\tau_{\rm A} = h_1/V_{\rm A}$, where $V_{\rm A}$ is the Alfvén velocity at the magnetic axis of FR1, the system is integrated in time for $100\ \tau_{\rm A}$. This reveals both the quality of the equilibrium and its unstable nature. Within the first $\sim 30\ \tau_{\rm A}$, the system attempts to settle to an exact numerical equilibrium from the approximate analytical one, with the velocities reaching a small peak and then falling to the very modest values of only $\approx 0.002\ V_{\rm A}$ in FR1 and $\approx -0.001\ V_{\rm A}$ in FR2, which indicates that the analytical equilibrium is nearly perfect. Subsequently, the velocities of both ropes begin to increase very gradually. This increase continues (roughly doubling the minimum values of the velocity by the end of the run), which indicates instability. By slightly modifying one of the currents, a nearly perfect equilibrium is found, with the residual velocities of FR1 falling monotonically to $1.4 \times 10^{-4}\ V_{\rm A}$ and the ones of FR2 oscillating very gradually around a value $6 \times 10^{-4}\ V_{\rm A}$ by $t = 100\ \tau_{\rm A}$; this requires reducing I_1 by 0.5%.

Next, this configuration is integrated for a range of $B_{\rm et}$ values, with a velocity perturbation applied at the apex of both flux ropes to find the minimum stabilizing external toroidal field. The velocity perturbation is applied for $5\ \tau_{\rm A}$, linearly ramped up to the peak value of $\pm 0.05\ V_{\rm A}$ and then switched off. Marginal stability (the critical value $B_{\rm et,\,cr}$) is found for $B_{\rm et}$ slightly below $1.7B_q$, with $B_{\rm et}$ and B_q taken at the lower flux rope's magnetic axis. Figure 2 shows field lines of the stable analytical equilibrium with $B_{\rm et} = 1.7B_q$ and of the configuration after numerical relaxation, along with height and velocity of the fluid elements at the apex points of the two flux ropes in the relaxation run. This stable numerical equilibrium is very close to the analytical one.

The external toroidal (shear) field strength required for stability is relatively high, exceeding the poloidal component of the external field (perpendicular to the filament). This situation can be realized on the Sun if the filament ends in the main flux concentrations of the active region. These sources then provide not only the axial field of the filament, but also give the ambient field a strong component in the direction of the filament. The filament investigated in Paper I did have this configuration.

2.2.2. *Unstable Configurations*

Full Eruptions — If the stabilizing external toroidal field strength is slightly reduced below the threshold value $B_{\rm et,\,cr} \approx 1.7B_q$, then the configuration can no longer be relaxed to a nearby equilibrium (Section 2.2.1). The nature of the instability and the complexity inherent in the configuration become apparent when $B_{\rm et}$ is reduced considerably. In this and the following two paragraphs we refer to simulations with $B_{\rm et} = B_{\rm et,\,cr}/3$ when quoting numbers. Identical qualitative behavior is obtained in the range $0 \le B_{\rm et} \lesssim B_{\rm et,\,cr}/2$. The simulations confirm that both flux ropes are unstable against vertical displacements (i.e., the torus instability) for the geometrical parameters chosen. The relevant parameter is the "decay index" of the total poloidal field at the position of each rope, $n = -d\ln(B_q + B_I)/d\ln h$, where B_I is the poloidal field from the other rope. Its threshold value lies in the range $n_{\rm cr} \approx 1.5$–2 if $B_{\rm et}$ is small (Kliem & Török 2006; Török & Kliem 2007). Our configuration yields $n_1 = 3.1$ and $n_2 = 2.8$, implying a higher growth rate for the instability of the lower flux rope FR1. (Additionally, higher Lorentz forces can be expected to develop in the evolution of the lower rope, since the field strength and current density are higher.) The decay index at the position of the lower flux rope generally has a high value, since the poloidal field of the upper flux rope, B_{I_2}, and the external poloidal field, B_q, are oppositely directed under the upper rope. The decay index at the position of the upper flux rope is largely determined by the field B_q, which has a supercritical decay index at heights exceeding $\sim L$. This condition is clearly met by our choice of geometrical parameters. Obviously, both flux ropes in a double flux rope equilibrium of the type studied in this paper tend to be torus unstable if the external toroidal (shear) field falls below the threshold value $B_{\rm et,\,cr}$.

Two different evolutions are enabled by the dominant insta-

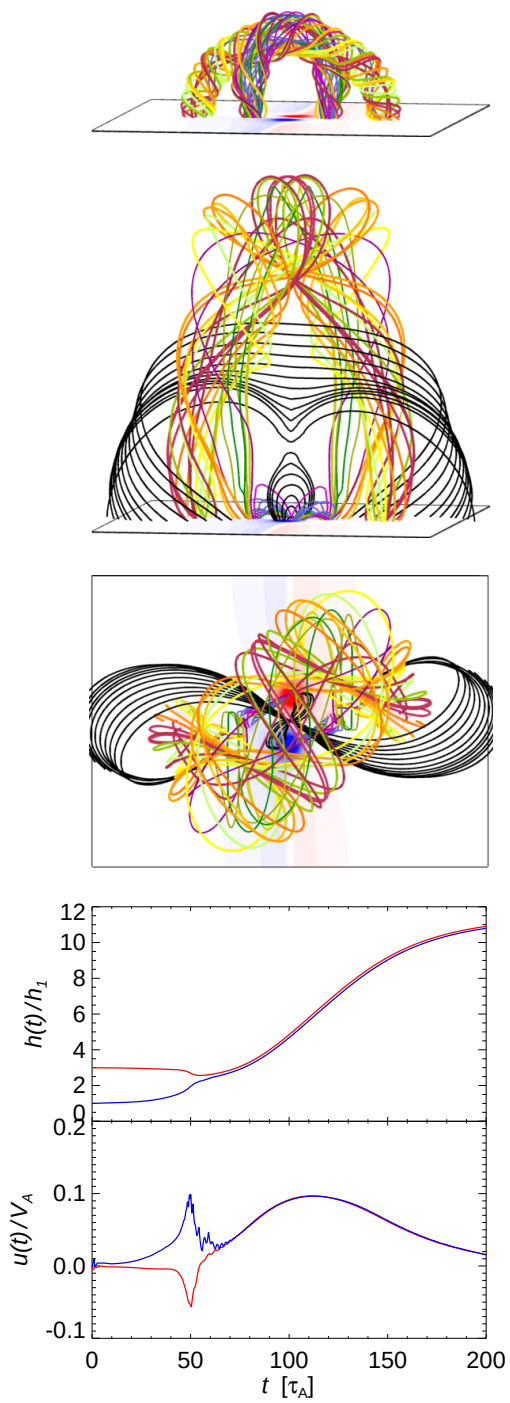

Figure 3. Instability and full eruption of the double flux rope equilibrium in the case of sub-critical external toroidal field, $B_{\rm et} = B_{\rm et,\,cr}/3$, and upward motion of the lower rope. Field line plots similar to Figure 2 are shown at $t = 65\ \tau_{\rm A}$ (top panel) and $t = 165\ \tau_{\rm A}$ (second and third panel). The lower flux rope largely merges with the upper one; the other part of its flux reconnects with the ambient flux to join the forming post-eruption arcade. The motion of the fluid elements at the apex points of the flux ropes is displayed in the bottom panel. A small upward initial velocity perturbation is applied at the apex of the lower flux rope.

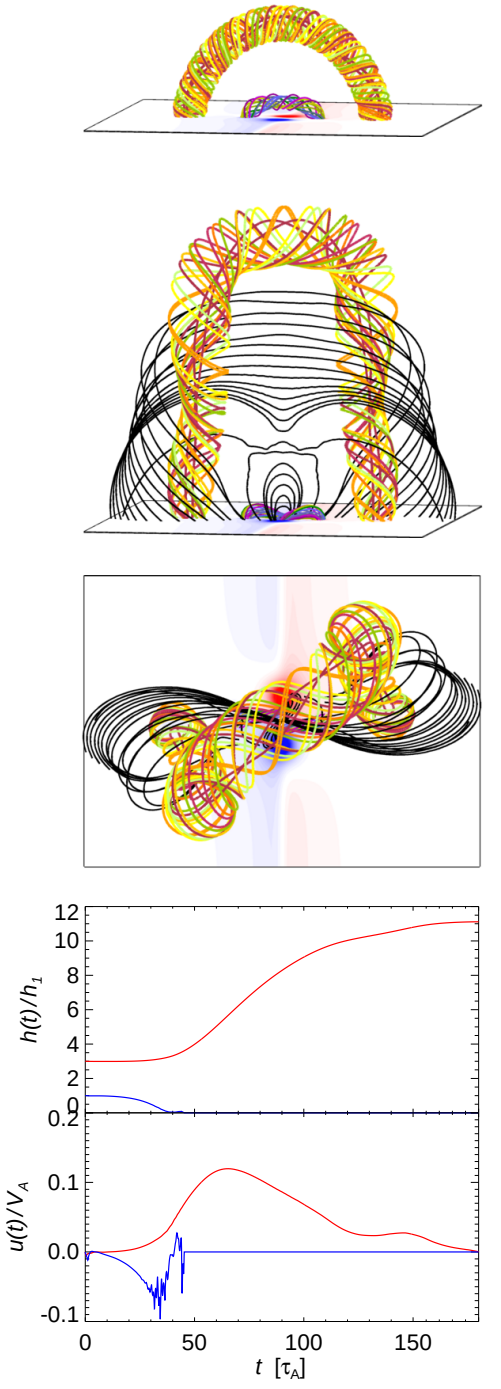

Figure 4. Same as Figure 3 for the case of downward moving lower rope (following a small downward velocity perturbation) at $t = 30\ \tau_{\rm A}$ (top panel) and $t = 100\ \tau_{\rm A}$ (second and third panel). Here all of the flux in the lower rope moves downward and reconnects with the ambient flux.

bility of the lower flux rope. When a small upward perturbation is applied to FR1, it then shows an exponential rise which saturates as the upper rope FR2 is approached. FR2 stays near its initial position in this period. Subsequently, the ropes merge, forming an arch which expands upward with a velocity of order $0.1\ V_{\rm A}$ (Figure 3). The rise is terminated at about four times the initial height of the upper rope, $h_2 = R_2 - d$, by the onset of reconnection between the legs of the strongly writhing rope and the ambient field. The writhing is here primarily due to the presence of $B_{\rm et}$ (Isenberg & Forbes 2007; Kliem et al. 2012), i.e., it does not indicate the development of the helical kink instability. The velocity doubles and the rise continues until the upper boundary of the box is approached if $B_{\rm et}$ is reduced further, below $\sim B_{\rm et,\,cr}/10$. This full eruption is clearly driven by the stronger torus instability of the lower flux rope and is very similar to the eruption of a single

torus-unstable flux rope.

When a small downward perturbation is applied to FR1, it shows a short, exponentially increasing downward displacement until the bottom boundary of the box (the model photosphere) is hit. FR1 then reconnects with the sunspot field, splitting in two low-lying ropes which come to rest at the bottom of the box. FR2 immediately begins an exponential rise which enters the saturation phase at about $1.5h_2$, followed by an approximately linear rise, again with a velocity of order $0.1\ V_{\rm A}$ (Figure 4). Similar to the case in Figure 3, reconnection between the legs of the writhing rope and the ambient field terminates the rise at $\sim 4h_2$, but a further reduction of $B_{\rm et}$ to $\sim B_{\rm et,\,cr}/10$ allows the upper flux rope to double the rise velocity and to escape (i.e., reach the top boundary of the box). Hence, a partial eruption (of only the upper flux rope) occurs, but it is accompanied by a strong change of the lower flux rope.

The scenario of decreasing $B_{\rm et}$ considered here may easily be realized on the Sun as the sources of the external toroidal field weaken by flux dispersal and cancellation. Thus, the eruption of double flux rope equilibria on the Sun will often involve a complete change of the configuration, both for full and partial eruptions. Since $B_{\rm et}$ will typically decrease only very gradually, the instability will set in long before a value of order $B_{\rm et,\,cr}/3$ is reached. Nevertheless, the upward directed velocities in such eruptions can be expected to be similar to or even higher than the values found in our simulations, since the external toroidal field in the corona is expected to fall off with height above the filament much faster than the model field, which is unrealistic in this regard (Section 2.1). The downward directed velocities should remain considerably below the simulated ones, since $B_{\rm et}$ will be much closer to the threshold value in this height range. Thus, in the scenario of eruptions enabled by gradually decreasing external toroidal field, a partial eruption may have a less dramatic effect on the lower flux rope than found in the simulation, but a destruction of the lower flux rope must still be expected. However, partial eruptions involving only the upper flux rope, with the lower flux rope remaining stable at its initial position, are also possible.

Partial Eruptions with a Stable Lower Flux Rope — A partial eruption can result under the same scenario of decreasing $B_{\rm et}$ if the upper flux rope is sufficiently twisted, so that the helical kink instability develops in the upper rope while the lower rope is still stable against the torus instability. We have verified this possibility by reducing the minor radius of the upper rope to $a_2 = 3.5$ Mm, which doubles its twist to about 10π, with $B_{\rm et}$ kept at the critical value of $1.7B_q$ of the original configuration. The upper rope then kinks upward, while the lower rope stays very close to its original position with very small residual velocity for more than $100\ \tau_{\rm A}$, i.e., apparently in a stable state. However, the occurrence of such high twist values is very unlikely and has so far been reported only in a single case (Romano et al. 2003). Therefore, we now consider another scenario for partial eruptions of double flux rope equilibria.

The observations analyzed in Paper I demonstrate that the most significant change in the energy buildup phase prior to the eruption consisted in the transfer of material and (necessarily current-carrying) flux from the lower to the upper branch of the filament (i.e., in the corona). To model this evolution, we next raise the current I_2 through the upper flux rope and decrease I_1 in the lower rope, keeping the total current $I_1 + I_2$ at the equilibrium value (and also $B_{\rm et} = 1.7B_q$). As a consequence, the HFT between the ropes moves a little bit downward, so that the cross sections and the total flux in the ropes experience a change similar to the currents. We have raised I_2 in small steps of $0.01I_2$ (with the corresponding changes of I_1 being close to $-\Delta I_2/2$) and found indications for the onset of instability of the upper rope at $\Delta I_2 = 0.04I_2$. For smaller changes of the currents both flux ropes relax very near their initial positions. For larger changes up to about $\Delta I_2 = 0.2I_2$, the lower flux rope still relaxes near its initial position, while the upper rope erupts.

This is shown in Figures 5 and 6 for the case $\Delta I_2 = 0.1I_2$. The upper rope FR2 first moves relatively quickly upward, to find the equilibrium position corresponding to the increased current $I_2 + \Delta I_2$ in about $30\ \tau_{\rm A}$. From this position, an approximately linear ascent to $\approx 1.5h_2$ commences. In the course of this rise, the left-handed rope writhes into a projected forward S shape, piling up a helical current sheet at its front side, analogous to the runs shown in Figures 3 and 4. Simultaneously, the HFT between the ropes collapses into a vertical current sheet. The upward outflow resulting from the onset of reconnection in this current sheet accelerates FR2 to a rise faster than linear ($t \gtrsim 650\ \tau_{\rm A}$). Since the overlying field resists the rise, primarily due to the relatively strong $B_{\rm et}$, the top part of the helical current sheet is quickly steepened and reconnection between FR2 and the overlying field commences at the rope apex, cutting the rope in two parts which remain confined. The lower flux rope FR1 is stabilized primarily by the external toroidal field, staying near the initial position for more than $10^3\ \tau_{\rm A}$ with velocities remaining smaller than the rise velocity of FR2 by a factor ~ 20. The terminal height of FR2 in Figure 6 is the result of reconnection with the overlying field. Overall the same behavior is found in the range $0.04 \leq \Delta I_2/I_2 \lesssim 0.2$, with the velocities increasing and reconnection commencing earlier for increasing ΔI_2.

To demonstrate that the rise of FR2 is driven by an instability, the run with $\Delta I_2/I_2 = 0.1$ is repeated with $B_{\rm et}$ reduced by a factor 10. Now the rise from the equilibrium position is initially relatively close to an exponential function, as expected for an instability developing in a weakly perturbed equilibrium (see Figure 6). (As discussed above, for this low value of $B_{\rm et}$ the lower flux rope FR1 is unstable as well.)

On the Sun, both the long-term stability of the double-decker filament and the ejective eruption of the upper branch into a CME can be allowed by an external toroidal field of the strength required for stability at the position of the filament, but falling off with height above the filament much faster than the model field. Our model field is unrealistic in this regard but the coronal field is generally expected to satisfy this condition (see, e.g., the modeling of an active region containing a filament in Su et al. 2011 and Kliem et al. 2013).

The transfer of flux from the lower to the upper flux rope is different from flux transfer by reconnection at the HFT between the ropes, e.g., tether-cutting reconnection. Such reconnection exchanges flux in both ropes with ambient flux. It is conceivable that the flux transfer is enforced by configuration changes of the current in the lower flux rope, which, in turn, can be enforced by changes in the photospheric boundary. It is well known that current-carrying flux rises if it is stressed by photospheric motions (e.g., Mikic & Linker 1994; Török & Kliem 2003). In the event considered in Paper I, the dominant photospheric change prior to the eruption consisted in the ongoing dispersion of the diffuse positive flux in the northern hook of the filament, which may have enforced an

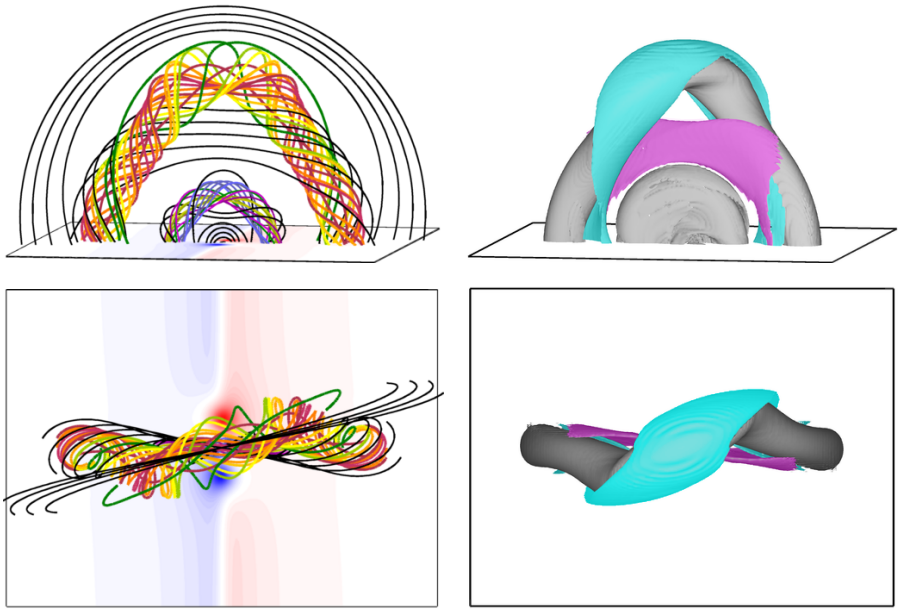

Figure 5. Partial eruption of the double flux rope equilibrium due to the instability of the upper rope after flux and current transfer from the lower rope ($\Delta I_2/I_2 = 0.1$) near the marginal stability condition in the absence of flux transfer, $B_{\rm et} = 1.7 B_q \gtrsim B_{\rm et,\,cr}$. Field lines similar to Figure 2 and current density isosurfaces at $|\mathbf{J}| = 0.07 J_{\rm max}$ show snapshots of the system at $t = 645\ \tau_{\rm A}$. The helical and vertical current sheets are colored in cyan and magneta, respectively. The ensuing reconnection of the unstable rope with the overlying field, which subsequently cuts the whole rope so that it remains confined in spite of the instability, is indicated by the dark green field lines.

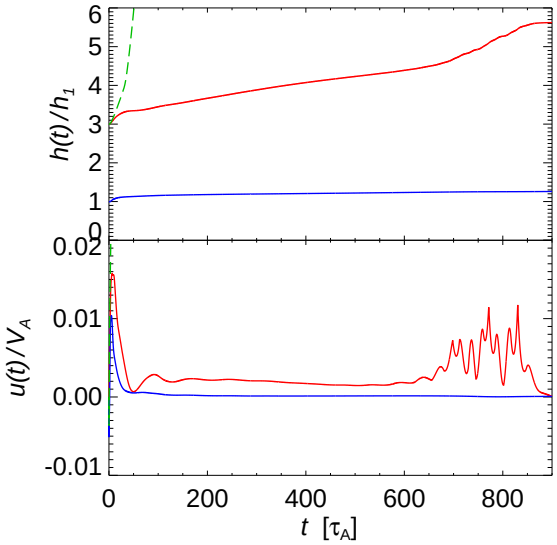

Figure 6. Height and velocity of the fluid elements at the apex points of the two ropes in the partial eruption shown in Figure 5, which does not employ any velocity perturbation. The dashed green lines show the rise of the unstable upper flux rope when $B_{\rm et}$ is reduced by a factor 10.

exchange of flux between the two filament branches. At the southern end of the filament, the moat flow of the negative sunspot moved flux in the direction from the end point of the lower branch to the end point of the upper branch (see Figure 2 in Paper I).

We have attempted to also model such driving by prescribing changes of the configuration only in the photospheric boundary. From each footpoint region of the lower rope, a patch of current-carrying flux was moved to the neighboring footpoint region of the upper rope by prescribing appropriate horizontal motions in the photosphere (satisfying symmetry with respect to the point under the flux rope apex). Although a number of different geometries for the path of the flux patch and different amounts of transferred flux were considered, none of the experiments succeeded in yielding a partial eruption as observed in the events analyzed in Paper I and Zhu & Alexander (2014). The perturbation always made both ropes unstable, with various combinations of upward and downward displacements of the ropes. FR1 was destroyed when moving downward and merged with FR2 when moving upward; the remaining/merged upper rope erupted in some runs and relaxed to an equilibrium at the new height otherwise. It appears that the generalized double Titov-Démoulin equilibrium is not appropriate for the modeling of such directly driven flux transfer between the ropes in their slow-rise phase because the ropes are too strongly twisted in their outer part. (The twist profile in the TD99 model increases toward the surface of the current channel in the rope; see Figure 2 in Török et al. 2004.) The flux bundle rooted in the moving photospheric flux patches, which originate from the surface of the lower current channel, winds considerably about the axis of the lower rope, so that the rope is always substantially perturbed. A less twisted, numerically constructed double flux rope equilibrium, like the one described in the following section or one obtained through the flux rope insertion method (e.g., Su et al. 2011), may allow the modeling of flux transfer driven at the photosphere with the lower rope remaining stable.

3. SPLITTING FLUX BUNDLE IN THE SLOW RISE PHASE OF A CME

The formation and partial eruption of a double flux rope configuration was also found in an MHD simulation that was designed to model the well-known filament eruption and CME on 1997 May 12 (e.g., Thompson et al. 1998; Webb et al. 2000). The details of this simulation will be described elsewhere (Linker et al., in preparation); here we merely summarize its main features and focus on the evolution shortly before the eruption.

The simulation code solves the standard resistive and viscous MHD equations on a spherical grid and incorporates radiative losses, thermal conduction parallel to the magnetic

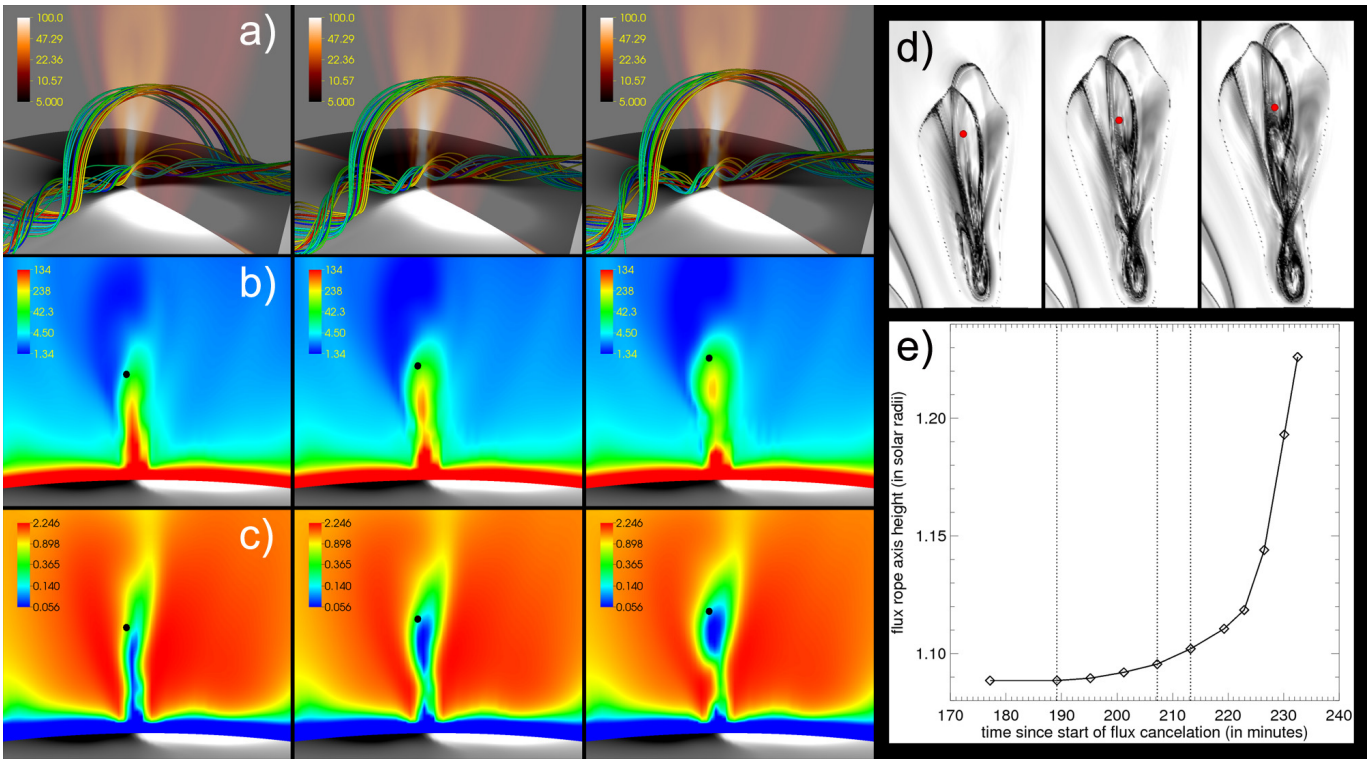

Figure 7. Snapshots of the 1997 May 12 simulation during the pre-eruptive phase. Panels (a–d): Vertical cuts perpendicular to the flux rope axis, taken at the apex of the upper rope; the specific times of the sub-panels from left to right are marked by dotted lines in the time-height profile of the upper flux rope axis apex shown in Panel (e). Panel (a) shows the (transparent) logarithmic distribution of the ratio of electric current density and magnetic field strength, j/B (in normalized units), and magnetic field lines that outline the cores of the upper and lower flux rope in an oblique view. Panels (b–d) are views along the upper flux rope axis, showing mass density ρ (in 10^{-16} g cm^{-3}), temperature T (in MK), and the logarithmic distribution of the squashing factor Q (shown in a zoomed view), respectively. The dots in panels (b–d) mark the approximative position of the upper flux rope axis apex. The radial magnetic field is shown in panels (a–c) at the photospheric plane, where white (black) colors outline strong positive (negative) flux.

field, and an empirical coronal heating function (see, e.g., Mikić et al. 1999; Lionello et al. 2009). The initial magnetic field in the simulation is obtained from a potential field extrapolation, using a combination of synoptic and real-time line-of-sight magnetograms (for a simplified model of the large-scale magnetic configuration around the time of the eruption, see Titov et al. 2008). After a solar wind MHD solution is obtained by relaxing the system to a steady state, the CME-producing active region is energized by a combination of photospheric shear flows and transverse field "emergence", which both keep the radial flux distribution unchanged (e.g., Linker et al. 2001; Bisi et al. 2010). This produces a highly sheared core field with little indications of twist, i.e., of flux rope geometry. Finally, the system is further energized, and an eruption is triggered, via flux cancellation, driven by localized flows converging toward the photospheric polarity inversion line (PIL) (e.g., Linker et al. 2003).

During the energization of the system, a sheet-like, coherent structure of cold and dense plasma forms within the core field (Figure 7(b),(c)). Interestingly, a significant fraction of this plasma is not located in concave-up field line segments, so the common picture of prominence material held against gravity in dipped fields does not seem to fully apply here. The detailed mechanisms by which this "prominence" is formed and maintained in the simulation require further study; both levitation of chromospheric plasma and condensation of coronal material may be involved. For our present purpose, it is sufficient to consider its evolution in the phase leading up to the eruption.

It has been shown that magnetic reconnection associated with flux cancellation successively transforms a sheared arcade into a flux rope, which slowly detaches from the photosphere, leaving behind short arched field lines (e.g., van Ballegooijen & Martens 1989; Amari et al. 2003; Aulanier et al. 2010). A similar process occurs in our simulation during the cancellation phase, although the evolution is more complex (Titov et al., in preparation). As can be inferred from vertical cuts of the so-called squashing factor Q (Titov et al. 2002), the core field consists of several flux bundles before it erupts (Figure 7(d)). The central flux bundle contains two adjacent flux ropes: a highly twisted low-lying one and an arched, less twisted upper one (Figure 7(a)). These two structures start to form relatively early in the cancellation phase, and gradually develop a flux rope geometry as they accumulate twist about their respective axes. However, in contrast to the distinct flux ropes considered in the previous subsection, a clear boundary between them does not develop; rather they remain merged to some extent for most of the cancellation phase. (Interestingly, although the upper flux rope possesses twist, it does not contain dipped field lines below its axis, which is due to its strong curvature.)

In the course of the flux cancellation and associated reconnection, the core field first expands quasi-statically until, after about 3.5 hours, its slow evolution transitions into a fast rise phase, marking the onset of the eruption (Figure 7(e)). In the pre-eruptive phase, the central flux bundle becomes increasingly stretched in the vertical direction. Shortly before the eruption, the splitting into two parts becomes more pronounced (Figure 7(d)), which is associated with tether-cutting reconnection of ambient flux into the core flux at the HFT be-

tween the two main flux bundles. The added flux runs under the apex of the upper flux rope and contributes to its twist, thus, it potentially acts destabilizing. For the lower rope, the added flux acts like strengthened overlying flux, thus stabilizing. The increasing separation of the flux ropes is accompanied by a splitting of the plasma sheet (Figure 7(b),(c)). Subsequently, the eruption carries away the upper flux rope and the top part of the plasma sheet, while the lower rope and the bottom part of the sheet remain at low heights.

The origin of the splitting of the central flux bundle must be different from the partial eruption mechanism modeled by Gibson & Fan (2006). There, the splitting of one coherent flux rope into two parts was associated with reconnection occurring in a current layer that formed in the course of the rope's eruption, due to a deformation (writhing) of the rope by the helical kink instability. In our case, the splitting occurs already in the pre-eruptive stage, during which no noticeable helical deformation takes place (Figure 7(a)). Moreover, two flux ropes form within the central flux bundle even earlier in the evolution. In a later simulation described in Fan (2010), where the eruption was driven by the torus instability, a current layer formed within the flux rope already in the pre-eruptive phase, and a similar breaking of the magnetic structure as in our simulation was observed (Y. Fan, private communication). Further study is required to fully understand how the splitting of the magnetic flux occurs in our simulation. A number of aspects may play a role, as for example the complexity of the initial potential field, the specific techniques by which the system is driven, gravity in regions of strong density, and reconnection at bald patches in the outer parts of the PIL.

By producing two stacked flux ropes early on in the evolution leading up to an eruption, our simulation supports the conjecture that such a configuration can exist in stable state for long periods in the corona, and it provides indications for their possible formation. Also, the splitting of the plasma sheet corresponds nicely to the observed separation of the two filament branches in the event analyzed in Paper I. However, the plasma splitting occurs only rather shortly before the eruption, different from the 2010 August 7 event (although the separation of the branches was most pronounced shortly before the eruption of the upper branch; see Figure 4 in Paper I). We did not succeed in producing a stable or longer-lasting configuration with a split plasma sheet by, for instance, switching off the flux cancellation at earlier times in the simulation. It seems that, at least for the specific parameters that were used to control the formation and driving of the core field in our simulation, such a configuration is difficult to obtain. The absence of plasma splitting at an earlier stage of the simulation might be due to the absence of field line dips in the upper flux rope. It remains to be seen whether the formation of (meta-)stable double-decker filament configurations can be modeled by simulations similar to the one presented here, or whether different physical mechanisms (as for example flux emergence) are required.

4. CONCLUSIONS

Stimulated by indications that vertically split ("double-decker") filaments and filament-sigmoid systems may form in double flux rope equilibria (Paper I; Zhu & Alexander 2014; Cheng et al. 2014), the present investigation shows that an approximate analytical equilibrium of two concentric, toroidal, force-free flux ropes can be constructed by a generalization of the methods developed in Titov & Démoulin (1999). The technique can be used for ratios of the major torus radii $R_2/R_1 \gtrsim 2.5$ and should be supplemented by numerical MHD relaxation to a nearby numerical equilibrium in the range $R_2/R_1 \lesssim 4$.

The equilibrium is stabilized by an external toroidal field $B_{\rm et}$ of sufficient strength, which can be considerable if the flux ropes are located relatively close to each other. For the geometry studied here, $R_2/R_1 = 2.5$ and the ratio of minor torus radii $a_2/a_1 = 1.5$, we find that $B_{\rm et} > B_{\rm et,\,cr} \approx 1.7 B_q$ is required, where B_q is the external poloidal field strength at the position of the inner (lower) flux rope.

The analytical construction of a double flux rope equilibrium with $B_{\rm et} \neq 0$ in this paper is restricted to the case that a line current at the symmetry axis of the tori is the source of $B_{\rm et}$. Therefore, $B_{\rm et}$ decreases only weakly with increasing distance R from the symmetry axis, $B_{\rm et} \propto R^{-1}$. This allows only confined eruptions to be modeled (except in the case that $B_{\rm et}$ is set considerably below $B_{\rm et,\,cr}$).

If the external toroidal field strength is reduced, then both flux ropes tend to become torus unstable. Typically the lower (inner) flux rope exhibits the stronger instability. This is due to the facts (*i*) that the poloidal field due to the upper (outer) flux rope is oppositely directed to the external poloidal field at the position of the lower flux rope, giving the total poloidal field at this position a steep decrease with height, and (*ii*) that field and current are generally stronger in the lower flux rope. If the lower flux rope erupts upward, it pushes the upper rope upward as well and merges with it. A full eruption of the configuration results which is quite similar to the eruption of a single flux rope. If the lower rope moves downward, it reconnects with the ambient field, splitting and coming to rest low in the box. This is accompanied by the upward eruption of the upper rope. However, it is also possible that only the upper flux rope turns unstable, with the lower rope staying in place without experiencing any significant change. This occurs in a scenario suggested by the observations in Paper I and Zhu & Alexander (2014) and demonstrated here: transfer of flux and current from the lower to the upper flux rope.

An equilibrium consisting of two force-free flux ropes, arranged vertically above a photospheric boundary, is also numerically obtained through an evolutionary sequence of shear flows, flux emergence, and flux cancellation in the photosphere. The stable double flux rope structure shows a slow rise in the cancellation phase. This evolution gradually transitions into a faster rise involving tether-cutting reconnection with the ambient field at the HFT between the ropes. Such reconnection lowers the stability of the upper flux rope and improves the lower rope's stability. Thus, it is a second potential driver for a partial eruption. The simulation indeed yields an eruption of the upper flux rope while the lower rope remains at low heights.

A third possibility, although less likely, consists in building up supercritical twist for onset of the helical kink instability only in the upper flux rope.

5. DISCUSSION

Both the existence of stable double flux rope equilibria and the possibility that only the upper flux rope loses stability support the suggestion that the split, partially erupting filaments investigated in Paper I and Zhu & Alexander (2014), and the filament-sigmoid systems investigated in Liu et al. (2010) and Cheng et al. (2014), may have formed in such a configuration.

This topology may not be a rare occurrence, since split filaments and prominences are seen quite frequently and since

partial eruptions are not uncommon (e.g., Pevtsov 2002). In hindsight rather many filament-sigmoid systems may be compatible with a double flux rope equilibrium, for example, the one in AR 10944, which partially erupted on 2007 March 2 (Sterling et al. 2007; Liu et al. 2008). The change of the originally discontinuous EUV sigmoid into a single continuous structure lying above the filament at the onset of this eruption is consistent with the tether-cutting reconnection between the flux ropes and the ambient field observed in the simulation in Section 3. One can expect a more general relevance also from the fact that the simulation in Section 3 was designed to model another event and yet shows a double flux rope. The existence of two flux ropes is quite likely in an event on 2010 March 30 which exhibits both confined and ejective components in a common eruption (Koleva et al. 2012). Both main branches of a split prominence were seen to erupt successively in an event on 2010 April 8 (Su et al. 2011), possibly providing an example for the case that the lower rope in a double flux rope equilibrium loses stability first. Moreover, the double flux rope topology may not only be relevant for split filaments and prominences, since one of the flux ropes, especially the upper one, may be void of absorbing material.

The episodic transfer of mass and magnetic flux to the upper branch of a split filament was found to be a likely destabilization mechanism for the upper branch in two events (Paper I and Zhu & Alexander 2014). Recently, such a "flux feeding" was observed to occur between chromospheric fibrils and an overlying filament, destabilizing the filament in an eruption on 2012 October 22 (Zhang et al. 2014). Thus, the transfer of mass and magnetic flux to a filament may be of more general relevance for the triggering of eruptions.

The support for the double flux rope configuration given here does not imply that the alternative configuration of a single flux rope situated above a magnetic arcade is less feasible. That configuration actually has advantages in terms of stability (it does not necessarily require a strong external shear field component to suppress instabilities), and it naturally allows partial eruptions that do not strongly perturb the lower part of the flux. However, it has the disadvantage that a basically different magnetic structure for the two filament branches is implied.

A formation mechanism for the double flux rope configuration in Figure 1(a) by the splitting of a coronal flux bundle driven by photospheric flows and flux cancellation has been demonstrated here (Section 3). A further mechanism is given by the emergence of a flux rope under an existing flux rope, as briefly discussed in Paper I. Additionally, the configuration may form in a generic manner in an extended period of flux cancellation, which first forms the configuration of Figure 1(b) and then produces the lower flux rope by acting on the arcade under the HFT.

Several new scenarios for partial eruptions are suggested by the investigations presented in Paper I and here. The upper part of a split flux system can erupt without strongly perturbing the lower part in the double flux rope configuration when only the upper flux rope is unstable (Figures 5–7), which can be achieved by flux transfer from the lower to the upper rope and by tether-cutting reconnection with the ambient field in the space between the ropes. Similar evolutions are possible in the configuration with a single flux rope separated by an HFT from an underlying arcade (Figure 1(b)). The double flux rope configuration also allows the eruption of the upper flux rope accompanied by downward motion and eventual destruction of the lower flux rope if the lower flux rope is unstable. In each of these cases, the flux can be split already during long periods before the eruption starts, in line with the properties of the filaments studied in Paper I and Zhu & Alexander (2014). This distinguishes them from the well known mechanism of a splitting unstable and line-tied flux rope in Gibson & Fan (2006) (see also Gilbert et al. 2001), which involves a splitting of the flux only in the course of the eruption.

B.K. acknowledges support by the DFG, the STFC, the NSF (grant AGS-1249270) and by the Chinese Academy of Sciences under grant 2012T1J0017. The contributions of T.T., V.S.T., R. Lionello, and J.A.L. were supported by NASA's HTP, LWS, and SR&T programs, and by CISM (an NSF Science and Technology Center). Computational resources were provided by NSF TACC in Austin and by NASA NAS at Ames Research Center. R. Liu, C.L., and H.W. were supported by NSF grants AGS-0849453, AGS-0819662, and AGS-1153226.

REFERENCES

Amari, T., Luciani, J. F., Aly, J. J., Mikic, Z., & Linker, J. 2003, ApJ, 585, 1073
Aulanier, G., Török, T., Démoulin, P., & DeLuca, E. E. 2010, ApJ, 708, 314
Bisi, M. M., Breen, A. R., Jackson, B. V., Fallows, R. A., Walsh, A. P., Mikić, Z., Riley, P., Owen, C. J., Gonzalez-Esparza, A., Aguilar-Rodriguez, E., Morgan, H., Jensen, E. A., Wood, A. G., Owens, M. J., Tokumaru, M., Manoharan, P. K., Chashei, I. V., Giunta, A. S., Linker, J. A., Shishov, V. I., Tyul'Bashev, S. A., Agalya, G., Glubokova, S. K., Hamilton, M. S., Fujiki, K., Hick, P. P., Clover, J. M., & Pintér, B. 2010, Sol. Phys., 265, 49
Cheng, X., Ding, M. D., Zhang, J., Sun, X. D., Guo, Y., Wang, Y. M., Kliem, B., & Deng, Y. Y. 2014, ApJ, in press; e-print arXiv1405.4923
Fan, Y. 2010, ApJ, 719, 728
Gibson, S. E., & Fan, Y. 2006, ApJ, 637, L65
Gilbert, H. R., Holzer, T. E., & Burkepile, J. T. 2001, ApJ, 549, 1221
Isenberg, P. A., & Forbes, T. G. 2007, ApJ, 670, 1453
Kliem, B., Su, Y. N., van Ballegooijen, A. A., & DeLuca, E. E. 2013, ApJ, 779, 129
Kliem, B., & Török, T. 2006, Phys. Rev. Lett., 96, 255002
Kliem, B., Török, T., & Thompson, W. T. 2012, Sol. Phys., 281, 137
Koleva, K., Madjarska, M. S., Duchlev, P., Schrijver, C. J., Vial, J.-C., Buchlin, E., & Dechev, M. 2012, A&A, 540, A127
Linker, J. A., Lionello, R., Mikić, Z., & Amari, T. 2001, J. Geophys. Res., 106, 25165
Linker, J. A., Mikić, Z., Lionello, R., Riley, P., Amari, T., & Odstrcil, D. 2003, Physics of Plasmas, 10, 1971
Lionello, R., Linker, J. A., & Mikić, Z. 2009, ApJ, 690, 902
Liu, C., Lee, J., Yurchyshyn, V., Deng, N., Cho, K., Karlický, M., & Wang, H. 2007, ApJ, 669, 1372
Liu, R., Gilbert, H. R., Alexander, D., & Su, Y. 2008, ApJ, 680, 1508
Liu, R., Kliem, B., Török, T., Liu, C., Titov, V. S., Lionello, R., Linker, J. A., & Wang, H. 2012, ApJ, 756, 59 (Paper I)
Liu, R., Liu, C., Wang, S., Deng, N., & Wang, H. 2010, ApJ, 725, L84
Mackay, D. H., Karpen, J. T., Ballester, J. L., Schmieder, B., & Aulanier, G. 2010, Space Sci. Rev., 151, 333
Mikic, Z., & Linker, J. A. 1994, ApJ, 430, 898
Mikić, Z., Linker, J. A., Schnack, D. D., Lionello, R., & Tarditi, A. 1999, Physics of Plasmas, 6, 2217
Pevtsov, A. A. 2002, Sol. Phys., 207, 111
Romano, P., Contarino, L., & Zuccarello, F. 2003, Sol. Phys., 214, 313
Roussev, I. I., Forbes, T. G., Gombosi, T. I., Sokolov, I. V., DeZeeuw, D. L., & Birn, J. 2003, ApJ, 588, L45
Savcheva, A., Pariat, E., van Ballegooijen, A., Aulanier, G., & DeLuca, E. 2012, ApJ, 750, 15
Shafranov, V. D. 1966, Reviews of Plasma Physics, 2, 103
Sterling, A. C., Moore, R. L., Berger, T. E., Bobra, M., Davis, J. M., Jibben, P., Kano, R., Lundquist, L. L., Myers, D., Narukage, N., Sakao, T., Shibasaki, K., Shine, R. A., Tarbell, T. D., & Weber, M. 2007, PASJ, 59, 823

Su, Y., Surges, V., van Ballegooijen, A., DeLuca, E., & Golub, L. 2011, ApJ, 734, 53
Thompson, B. J., Plunkett, S. P., Gurman, J. B., Newmark, J. S., St. Cyr, O. C., & Michels, D. J. 1998, Geophys. Res. Lett., 25, 2465
Titov, V. S., & Démoulin, P. 1999, A&A, 351, 707
Titov, V. S., Hornig, G., & Démoulin, P. 2002, J. Geophys. Res., 107, 1164
Titov, V. S., Mikic, Z., Linker, J. A., & Lionello, R. 2008, ApJ, 675, 1614
Török, T., & Kliem, B. 2003, A&A, 406, 1043
—. 2005, ApJ, 630, L97
—. 2007, Astron. Nachr., 328, 743
Török, T., Kliem, B., & Titov, V. S. 2004, A&A, 413, L27
van Ballegooijen, A. A., & Martens, P. C. H. 1989, ApJ, 343, 971
Webb, D. F., Lepping, R. P., Burlaga, L. F., DeForest, C. E., Larson, D. E., Martin, S. F., Plunkett, S. P., & Rust, D. M. 2000, J. Geophys. Res., 105, 27251
Zhang, Q., Liu, R., Wang, Y., Shen, C., Liu, K., Liu, J., & Wang, S. 2014, ApJ, in press; e-print arXiv1405.6833
Zhu, C., & Alexander, D. 2014, Sol. Phys., 289, 279